2017 14th International Conference on Ubiquitous Robots and Ambient Intelligence (URAI)
June 28 - July 1, 2017 at Maison Glad Jeju, Jeju, Korea

Design Parameter Optimization of a Novel Serial Manipulator for Microsurgery

Byungchul An[1], Woosub Lee[2], Sungchul Kang[2], Chunwoo Kim[2]
[1]School of Mechanical Engineering, Seoul National University, Seoul, Korea
(Tel : +82-2-880-7149; E-mail: abc8512@snu.ac.kr)
[2]Healthcare Robot Group, Korea Institute of Science and Technology, Seoul, Korea
(Tel : +82-2-958-6836; E-mail: cwkim@kist.re.kr)

***Abstract*—Surgical robots for microsurgery have mostly been continuum robot type. We present a new serial robot type manipulator for microsurgery, AsclRod. The manipulator consists of a stiff, slim tubes connected by rotation-prismatic joints. Being a serial robot, the manipulator provides improved stiffness and tractable kinematics compared to previous continuum robot type manipulators.**

Performance index of the manipulator is defined in terms of the workspace size, insertion port diameter, and tip orientation dexterity. Design parameters of each link of the manipulator are optimized to maximize the performance index while satisfying the constraint of the target application, endonasal skull base surgery (ESBS).

***Index Terms*—Surgical Robot, Microsurgery, Manipulator Design Optimization.**

I. Introduction

Many robot systems have been developed to assist surgery and currently, the commercial surgical robot systems are mostly used for laparoscopic surgery (daVinci) and orthopaedics (ROBODOC). Microsurgeries - surgeries in smaller scale in field of neurosurgery, ophthalmology and ENT - can benefit from the precision and dexterity of robot manipulation, but has not been yet explored.

One of the challenges in the microsurgical robot is development of a manipulator that is slim enough to enter through the narrow passages of the body, while being steerable for navigation through body lumen and dexterous manipulation of the surgical tool, and yet stiff enough to endure large loads during tissue manipulation. Development of such 3S (slim, steerable and stiff) manipulator remains as a big challenge in the advancement of microsurgical robots.

Many manipulators developed for microsurgery [1], [2], [3] has been based on continuum robots, which relies on the deformation of an elastic element to generate the manipulator motion. Continuum robots have fundamental limitation in stiffness and its kinematics is based on solution of beam deflection boundary value problems, leading to complicated and imprecise kinematics.

In this paper, we present a novel serial manipulator for microsurgery, which consists of series of slim rigid tubes connected by revolute-prismatic (RP) joints. The manipulator has high stiffness as its link is made of rigid SUS tube and has analytic kinematic solution as the structure is serial. We describe basic structure of the manipulator and formulate its kinematics. Then, we define performance index of the manipulator considering the workspace size, insertion port diameter, and tip orientation dexterity. Finally, the design parameters of each link of the manipulator are optimized to maximize the performance index while satisfying the constraint of the target application, endonasal skull base surgery (ESBS).

II. AsclRod Model

The new serial manipulator consists of three links serially connected by revolute-prismatic (RP) joint as shown in Fig. 1a. Each link is made of curved tube with straight segments at both ends as shown in Fig. 1b. When the links are assembled, the straight segment of the neighboring tubes overlap and forms the RP joint. These joints are driven by torque coils delivered through the lumen of the tube. Shape of the assembled manipulator resembles the rod of Asclepius - god of medicine in Greek mythology - and the manipulator is named AsclRod.

In terms of 3S (slim, stiff, steerable) requirement of microsurgical robot, being a serial robot, AsclRod can provide greater stiffness and steerability compared to other microsurgical robot [2], [3] that are continuum robot. In terms of stiffness, as it does not rely on the deformation of the elastic element for the actuation, AsclRod can provides greater stiffness by using stiff material such as stainless steel tube for its body. Being a serial manipulator, AsclRod provides analytical solution for forward and inverse kinematics, making it easier to control and provides advantage in terms of steerability. Finally, AsclRod is slim as it consists of slender tubes.

In next subsections, we formulate the forward kinematics of the manipulator, and using the formulated kinematics, analyze the workspace, orientation dexterity, and minimum insertion diameter configuration of the AsclRod.

A. Kinematics

Since the AsclRod is a serial manipulator, its forward kinematics can be easily formulated by concatenating transformation matrices. For this, coordinate systems A_i and B_i are attached to the base and tip of the each i^{th} link, respectively, as shown in Fig. 1b. The coordinate systems are attached such that the Z axes of both coordinate systems are tangent to the centerline of the tube.

978-1-5090-3056-9/17/$31.00 ©2017 IEEE

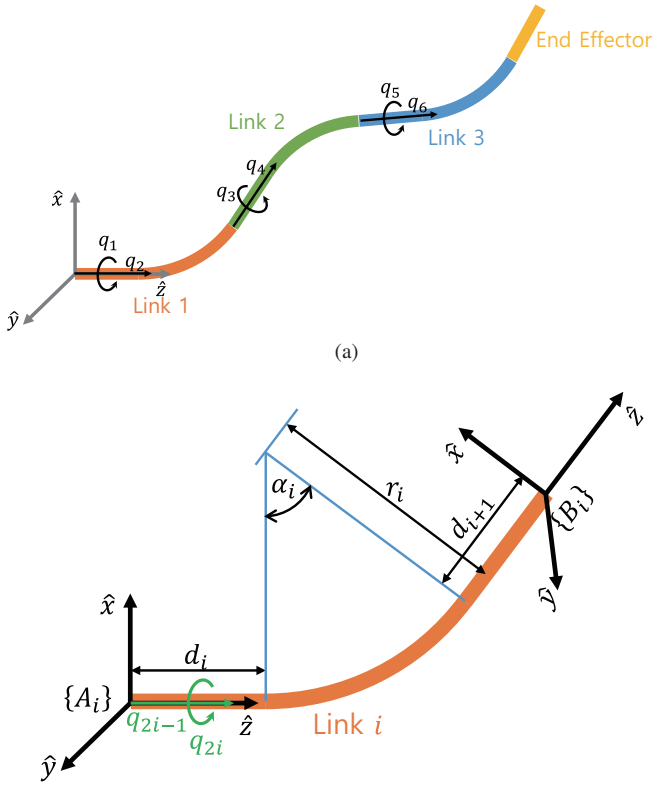

Fig. 1: Structure of (a) AsclRod and (b) one of its link.

The prismatic joints and revolute joints are attached at the base of each link along the Z axis and translates and rotates the tube by q_{2i-1} mm and q_{2i} degree, respectively. Then, the configuration of the tip coordinate system with respect to the base coordinate system is

$$ {}^{A_i}_{B_i}T_i(q_{2i-1}, q_{2i}) = \begin{bmatrix} R_{2i} & \mathbf{z}_{2i-1} \\ \mathbf{0^T} & 1 \end{bmatrix} \begin{bmatrix} X_i & \mathbf{t}_i \\ \mathbf{0^T} & 1 \end{bmatrix} \tag{1} $$

where R_i is rotation matrix representing the rotation about Z axis by angle q_i and $\mathbf{z}_i = [0, 0, q_i]^T$. X_i and $\mathbf{t_i}$ are initial orientation and position of the B_i with respect to A_i at zero joint angle, which are determined by the link design. In this paper, the shape of the link is restricted to circular arc, hence, the design parameters of the links are length of the straight segment $\bar{d} = [d_1, d_2, d_3, d_4]$, radius of circular arc $\bar{r} = [r_1, r_2, r_3]$, and angle of circular arc $\bar{\alpha} = [\alpha_1, \alpha_2, \alpha_3]$ as shown in Fig. 1b.

The links are assembled in a way that at the initial configuration, coordinate system A_i and B_{i-1} coincide, as shown in Fig. 1a. Then the configuration of the robot tool tip coordinate system (coordinate system B_3) as a function of joint angles $\mathbf{q} = [q_1, q_2, \cdots, q_6]^T$ is

$$ \begin{aligned} T &= \begin{bmatrix} R_2 & \mathbf{z_1} \\ \mathbf{0^T} & 1 \end{bmatrix} \begin{bmatrix} X_1 & \mathbf{t_1} \\ \mathbf{0^T} & 1 \end{bmatrix} \begin{bmatrix} R_4 & \mathbf{z_3} \\ \mathbf{0^T} & 1 \end{bmatrix} \\ &\quad \begin{bmatrix} X_2 & \mathbf{t_2} \\ \mathbf{0^T} & 1 \end{bmatrix} \begin{bmatrix} R_6 & \mathbf{z_5} \\ \mathbf{0^T} & 1 \end{bmatrix} \begin{bmatrix} X_3 & \mathbf{t_3} \\ \mathbf{0^T} & 1 \end{bmatrix} \qquad (2) \\ &= \begin{bmatrix} R & \mathbf{p} \\ \mathbf{0^T} & 1 \end{bmatrix} \qquad (3) \end{aligned} $$

Expanding the above equation, orientation R and position p of the tool is

$$ \begin{aligned} R &= R_2X_1R_4X_2R_6X_3 \qquad (4) \\ \mathbf{p} &= \mathbf{z_1} + R_2X_1\mathbf{z_3} + R_2X_1R_4X_2\mathbf{z_5} + \\ &\quad R_2\mathbf{t_1} + R_2X_1R_4\mathbf{t_2} + R_2X_1R_4X_2R_6\mathbf{t_3}. \qquad (5) \end{aligned} $$

III. Performance Index

In order to optimize design parameters, first we define several performance indices. The performance indexes have been defined based on the functionality of a manipulator as a surgical robot. First, the tip of the manipulator should be able to reach everywhere within a target surgery workspace. Second, at each point within the workspace, manipulator should be capable of orienting the tool tip in wide range of direction. Finally, entire manipulator should be slim enough to pass through narrow entry port.

A. Workspace

Workspace is defined as a region that can be reached by the tool tip of the AsclRod, regardless of the tip orientation. As can be seen from the structure of the robot, (Fig. 1a), its workspace will have rotational symmetry about Z-axis. Therefore, it is sufficient to find the cross section of the workspace in ZX-plane.

Given the design parameters, from the forward kinematics Eq. (5) and using the rotational symmetry, position of end effector can be rewritten as

$$ \mathbf{p} = \begin{bmatrix} p_x(\mathbf{q}) \\ p_y(\mathbf{q}) \\ p_z(\mathbf{q}) \end{bmatrix} = \begin{bmatrix} r\cos\theta \\ r\sin\theta \\ z \end{bmatrix}. \tag{6} $$

First, we find the range of $z \in [z_{min}, z_{max}]$ that end effector can reach by solving following two optimization problems over the joint angle under constraint of joint angle range

$$ \begin{aligned} z_{min}^2 &= \min_{\mathbf{q}} {p_z}^2 \qquad (7) \\ z_{max}^2 &= \min_{\mathbf{q}} -{p_z}^2. \qquad (8) \end{aligned} $$

Then, the calculated range of z is discretized in 1 mm interval, and for each discretized point $z_c \in [z_{min}, z_{max}]$, we find minimum and maximum distance r from Z-axis by solving similar optimization problems,

$$ \begin{aligned} r_{min}^2 &= \min_{\mathbf{q}} (p_x^2 + p_y^2) \quad s.t. \quad p_z(\mathbf{q}) = z_c \qquad (9) \\ r_{max}^2 &= \min_{\mathbf{q}} -(p_x^2 + p_y^2) \quad s.t. \quad p_z(\mathbf{q}) = z_c. \qquad (10) \end{aligned} $$

Example cross section of workspace is shown in Fig. 2.

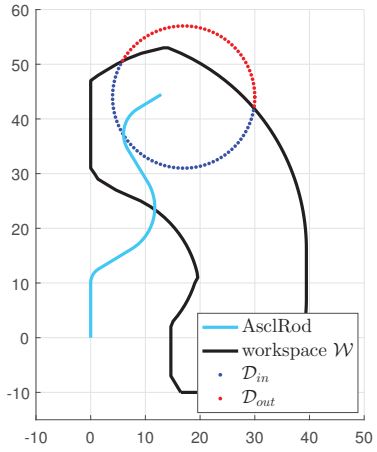

Fig. 2: Cross section of the robot workspace (black line) and target workspace (circle) in ZX-plane.

B. Orientation Dexterity

During the manipulation of the surgical tools, suturing for example, it is important for the AsclRod to be able to pivot the tool about a fixed position and orient it in multiple directions. In this section we describe analytic procedure for finding the range of pointable tool tip direction at a given end effector position to quantify the orientation dexterity of the AsclRod.

Tool tip direction is the direction of Z axis of the tip coordinate system B_3 of the 3rd link. This tip direction can be parametrized by spherical coordinate as $[\sin\phi\cos\theta, \sin\phi\sin\theta, \cos\phi]^T$ and then the orientation of the tool coordinate system can be parametrized in ZYZ Euler angle as below,

$$R = R_2X_1R_4X_2R_6X_3 = Z_\theta Y_\phi Z_\psi \tag{11}$$

with the last rotation by ψ being the redundant rotation about the tool tip direction, Then, the range of the pointable tool tip direction is defined as a range of θ and ϕ that can be achieved while maintaining the tip position at $\mathbf{p}$ and satisfying the joint limit of the prismatic joints q_1, q_3 and q_5. This range is identified by the following procedure.

First, the range of ϕ and q_6 is discretized. Then for each value of ϕ and q_6, the range of θ that satisfies the constraint of tip position and joint limit is calculated. This range of θ calculated for each value of q_6 is merged to obtain $[\theta_{min}, \theta_{max}]$ for each ϕ. Algorithms are summarized in Algorithm 1.

Details are as follows.

1) find q_4: From Eq. (11), multiplying $\hat{z} = [0,0,1]^T$ to both side and using the fact that $\hat{z}$ is invariant by rotation about z axis

$$\hat{z}^TR_2X_1R_4X_2R_6X_3\hat{z} = \hat{z}^TZ_\theta Y_\phi Z_\psi\hat{z} \tag{12}$$

$$p^TR_4q = \cos\phi \tag{13}$$

where $p = \hat{z}^TX_1, q = X_2R_6X_3\hat{z}$. Eq. (13) can be expanded and solved to give maximum two solutions for q_4 for given q_6 and ϕ.

Algorithm 1 FindPointableRegion

```
For φ_i ∈ [0, π]
  For q_6j ∈ [0, 2π]
    q_4 ← findq_4(φ_i, q_6j)
    [q_2^min, q_2^max] ← findRangeq_2(φ_i, q_4, q_6j)
    [θ_ij^min, θ_ij^max] ← findRangeθ(q_2^min, q_2^max)
  end
end
return [φ_min, φ_max], [θ_min, θ_max]
```

2) findRange q_2: Eq. (5) which defines the tool tip position, can be rearranged as

$$R_2^T\mathbf{p} = A\begin{bmatrix} q_1 \\ q_3 \\ q_5 \end{bmatrix} + \gamma \tag{14}$$

where

$$A = \begin{bmatrix} \hat{z} & X_1\hat{z} & X_1R_4X_2\hat{z} \end{bmatrix} \tag{15}$$

$$\gamma = \mathbf{t_1} + X_1R_4\mathbf{t_2} + X_1R_4X_2R_6\mathbf{t_3}. \tag{16}$$

With q_6, q_4 and ϕ fixed, A and γ can be evaluated and the prismatic joint angles $[q_1, q_3, q_5]^T$ must satisfy

$$\begin{bmatrix} q_1^{\min} \\ q_3^{\min} \\ q_5^{\min} \end{bmatrix} \le \begin{bmatrix} q_1 \\ q_3 \\ q_5 \end{bmatrix} = A^{-1}(R_2^T\mathbf{p} - \gamma) \le \begin{bmatrix} q_1^{\max} \\ q_3^{\max} \\ q_5^{\max} \end{bmatrix} \tag{17}$$

Solving the system of inequalities Eq. (17) gives the admissible range of q_2. Finally the range of achievable θ can be calculated from

$$R_2X_1R_4q = [\sin\phi\cos\theta, \sin\phi\sin\theta, \cos\phi]^T \tag{18}$$

Step 1) and 2) are repeated for sets of $[\phi, q_6]$ to find range of θ for each ϕ.

Given the range of $[\phi, \theta]$, dexterity is calculated as a ratio of pointable region on the surface of a unit hemisphere centered at a given end effector position.

$$M_{\text{DEX}} = \frac{1}{2\pi} \times \int_A \sin\phi d\theta d\phi \tag{19}$$

where M_{DEX} stands for dexterity measure, and A is the range of the (θ, ϕ). This is normalized by the area of unit hemisphere 2π.

C. Minimum Insertion Port Diameter

While individual link of the AsclRod is made of slim tubes, the assembled AsclRod will not be as slim as the individual link, and the diameter of the port that AsclRod can pass through will vary depending on the joint configuration of the AsclRod. Therefore, it is necessary to find out the smallest port diameter that AsclRod can pass through and the joint angle configuration that achieves this minimum insertion port diameter.

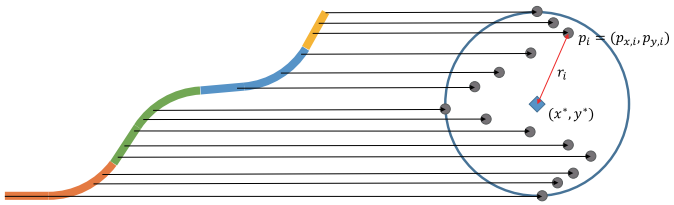

Fig. 3: Insertion diameter of AsclRod. Left figure is the projection of AsclRod in XZ-plane. Right figure is the projection on XY-plane (view on Z axis).

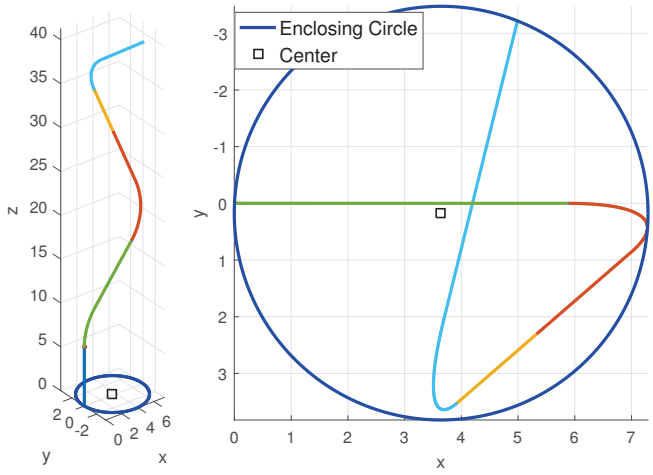

Fig. 4: A case study of minimum enclosing circle. Left figure is entire shape of AsclRod and Right is projection view. Design parameteres are $\alpha = [37, 55, 72]^\circ$, $r = [6.75, 6.75, 3.75]mm$, $d = [6.75, 7.5, 6, 6.75]mm$.

As shown in Fig. 3, AsclRod is inserted in Z-direction and the diameter of a circle that encloses the projection of the whole links onto XY-plane is the required insertion port diameter at that configuration. Finding size of this diameter can be shown as minimum enclosing circle problem which is studied in previous literatures [4], [5], [6], [7]. The problem is kind of minimax optimization problem. For a set of points $I = \{p_i | p_i = (x_i, y_i), i = 1, \cdots, N\}$, the objective is to solve following optimization problem

$$(x^*, y^*) = \arg\min_{x,y} \max_{p_i \in I} r \tag{20}$$

where $r = \sqrt{(x - p_{i,x})^2 + (y - p_{i,y})^2}$, and I is set of discretized link points of AsclRod at given arbitrary configuration. Algorithms for solving above optimization problem is well studied in previous literatures.

In order to find the configuration that minimize the insertion port diameter, we reformulate Eq. (20) above as

$$\mathbf{q}^* = \arg\min_{\mathbf{q}} \min_{x,y} \max_{p_i \in I} r \tag{21}$$

where $r = \sqrt{(x - p_{i,x}(\mathbf{q}))^2 + (y - p_{i,y}(\mathbf{q}))^2}$. Now r becomes a function of joint configuration $\mathbf{q}$. To solve the problem Eq. (21), we use particle swarm optimization (PSO) [8]. In every iteration of PSO algorithm, optimization solver generate samples (called particles) and solves optimization sub problem Eq. (20). A case study of minimum insertion port diameter calculation is shown in Fig. 4. It shows that the joint configuration that minimizes the insertion port diameter can be non trivial.

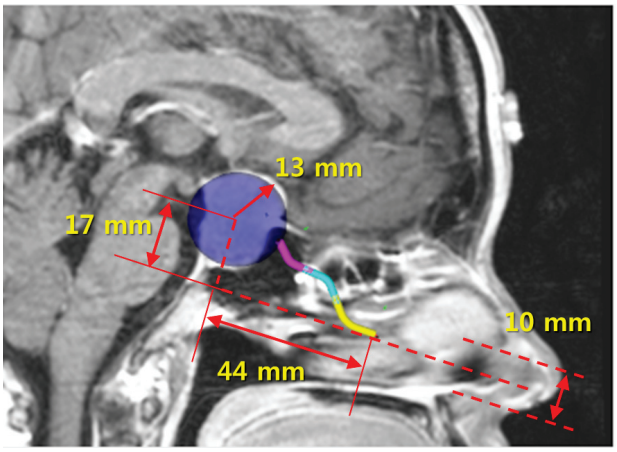

Fig. 5: Target workspace and insertion port constraint in ESBS

IV. Design Parameter Optimization

In this section, design parameters of the AsclRod are optimized to satisfy the requirement of its target microsurgery, endonasal skull base surgery (ESBS). ESBS is an surgical procedure where the tools are delivered through the nostril to access the skull base and remove tumor. Fig 5 shows the typical tumor location and tool access direction in the ESBS. The tumors are located in the region offset from the tool insertion direction. Hence the target workspace can be modelled as a 13 mm radius sphere centered at (17,0,44) in robot coordinate system, and the insertion port size should be less than 10 mm. We would like to maximize dexterity while satisfying these workspace and insertion port constraints.

For this, we defined cost function combining the performance indices defined in the previous section - workspace, orientation dexterity and minimum insertion port diameter - and performed the optimization of the design parameters α, r. Since the performance indices are complicated nonlinear functions of the design parameters whose gradient are cannot be explicitly calculated, particle swarm optimization algorithm is used for the optimization.

A. Cost Functions

The cost function for the design parameter optimization was defined as

$$J = J_{\text{WS}} + J_{\text{DEX}} + J_{\text{ID}} \tag{22}$$

where $J_{\text{WS}}, J_{\text{DEX}}, J_{\text{ID}}$ are cost functions for workspace, orientation dexterity, and minimum insertion diameter. Definition of each cost function is as follows.

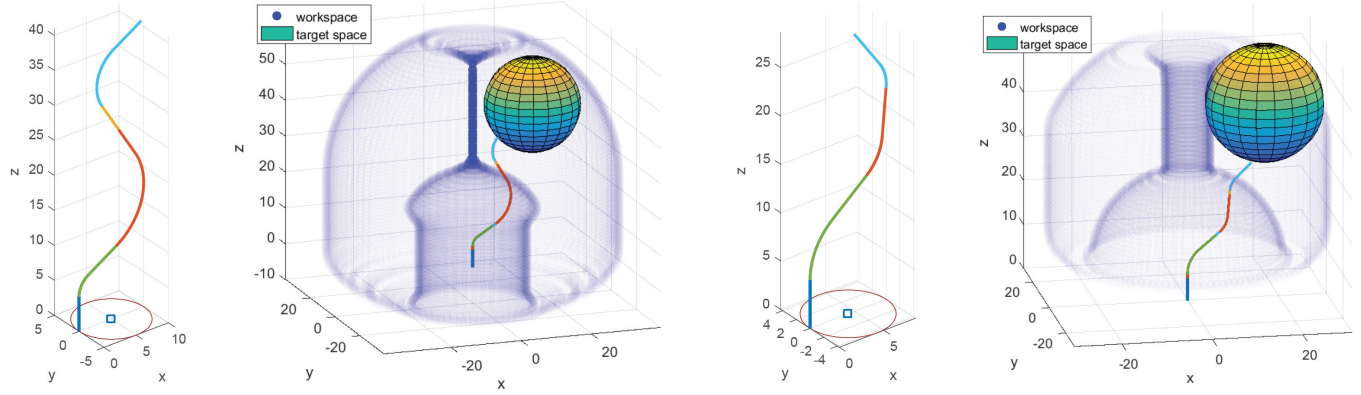

Fig. 6: Comparison of minimum insertion port diameter and workspace for optimized design parameters (a and b) and reference design parameter (c and d)

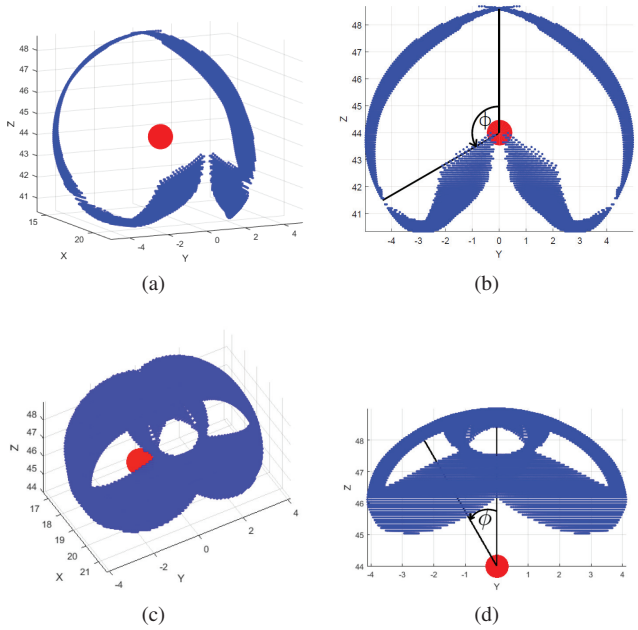

Fig. 7: Range of the tip directions achievable from the center of the workspace (red circle). a) Perspective and b) YZ-plane view of the range for optimized design parameters. c) Perspective and d) YZ-plane view of the range for reference design parameters.

TABLE I: Optimization Result

		optimal	reference
Design Parameters	$\alpha(^\circ)$	$[58.77, \quad 90.00, \quad 90.00]$	$[50, \quad 45, \quad 40]$
	$r(mm)$	$[3.00, \quad 8.91, \quad 5.43]$	$[7, \quad 5, \quad 4]$
Cost	J	-2.30	-1.25
	J_{WS}	-1	$-7.78e^{-20}$
	J_{DEX}	-0.30	-0.25
	J_{ID}	-1.00	-1
Minimun Insertion Port Diameter (mm)		10.0	8.6

1) Workspace: From the cross section of the robot workspace $\mathcal{W}$ and the target workspace $\mathcal{T}$ for the ESBS in ZX-plane shown in Fig. 2, the boundary $\partial\mathcal{W}$ and $\partial\mathcal{T}$ of each workspace is discretized to set of points $P(\mathcal{D}_{\text{ws}})$ and $P(\mathcal{D}_{\text{target}})$. The cost function J_{WS} for the robot workspace is calculated from the number of points $\mathcal{N}(\mathcal{D}_{\text{out}})$ in $P(\mathcal{D}_{\text{target}})$ that lies outside $\mathcal{W}$ (red segment in Fig. 2).

$$J_{\text{WS}} = -\exp\left(-\mathcal{N}(\mathcal{D}_{\text{out}})\right). \tag{23}$$

2) Orientation Dexterity: Evaluating the dexterity measure defined in equation (19) at every point within the target workspace is computationally intractable. Therefore, the dexterity measure at the center of the target workspace was used to evaluate the cost function J_{DEX}.

$$J_{\text{DEX}} = -M_{\text{DEX}}. \tag{24}$$

3) Minimun Insertion Diameter: Given the insertion port size requirement $D \leq D_{\text{req}}$, the cost function for minimum insertion port size is calculated by

$$J_{\text{ID}} = \begin{cases} (D - D_{\text{req}})^2 - 1 & \text{for} \quad D \geq D_{\text{req}} \\ -1 & \text{for} \quad D < D_{\text{req}} \end{cases} \tag{25}$$

B. Optimization Result and Discussion

As shown in Fig. 5, the target workspace was defined as a sphere centered at $[17, 0, 44]$ with radius 13. The insertion port size requirement was $D \leq D_{\text{req}} = 10$. The boundary of the design parameter r_i and α_i was set to be $\alpha_i \in [0, \frac{\pi}{2}], r_i \in [3, 10], i = 1, 2, 3$. The length of the straight segment of each tube d_i was fixed to 5 mm and the limit of the prismatic joints was set to be $q_1 \in [0, 20], q_3, q_5 \in [0, 5]$.

Table I shows the optimized design parameter and compares it with the arbitrarily selected reference design parameter. For both design parameters, the performance measures of the AsclRod are visualized in Fig. 6 and 7. In terms of workspace and minimum insertion port diameter, AsclRod with the optimized design parameter completely covers the target workspace while satisfying the insertion port diameter limit $D \leq D_{\text{req}} = 10$, as shown in Fig. 6.

In terms of the orientation dexterity, Fig. 7 shows that the range of the ϕ in tip direction $[\sin\phi\cos\theta, \sin\phi\sin\theta, \cos\phi]^T$ parametrized by spherical coordinate, is greatly increased as a result of the optimization. The range of ϕ in optimized AsclRod exceeds $90°$, indicating that with the optimized design parameters, the AsclRod can even point tool tip backward. However, considering that surgery usually requires manipulation of the objects that are in front of the tool, such a large range of orientation may not be necessary, and the range of ϕ should be limited (below $90°$) during optimization in future research.

V. Conclusion

In this paper, we present AsclRod, a novel serial manipulator for microsurgery. The serial structure of the robot can provide increased stiffness and simple kinematics compared to the previous microsurgical robots based on continuum robot. The design parameters of the robot was optimized to satisfy the requirement of target workspace, orientation dexterity and minimum insertion port diameter for its intended application, ESBS. While the optimized design shows that feasible structure of the AsclRod exists for ESBS, it remains as a future work to physically implement the AsclRod with the optimized design. Fabrication of the tubes with high curvatures, precise control of each link via actuation delivered by torque coils are some of the technical challenge that will be addressed as we move forward to build a working AsclRod robot.

References

[1] J. Burgner-Kahrs, D. C. Rucker, and H. Choset, "Continuum robots for medical applications: A survey," *IEEE Transactions on Robotics*, vol. 31, no. 6, pp. 1261–1280, Dec 2015.

[2] J. Burgner, D. C. Rucker, H. B. Gilbert, P. J. Swaney, P. T. Russell, K. D. Weaver, and R. J. Webster, "A telerobotic system for transnasal surgery," *IEEE/ASME Transactions on Mechatronics*, vol. 19, no. 3, pp. 996–1006, June 2014.

[3] A. H. Gosline, N. V. Vasilyev, E. J. Butler, C. Folk, A. Cohen, R. Chen, N. Lang, P. J. del Nido, and P. E. Dupont, "Percutaneous intracardiac beating-heart surgery using metal mems tissue approximation tools," *The International Journal of Robotics Research*, vol. 31, no. 9, pp. 1081–1093, 2012.

[4] S. K. Jacobsen, "An algorithm for the minimax weber problem," *European Journal of Operational Research*, vol. 6, no. 2, pp. 144–148, 1981.

[5] D. W. Hearn and J. Vijay, "Efficient algorithms for the (weighted) minimum circle problem," *Operations Research*, vol. 30, no. 4, pp. 777–795, 1982.

[6] N. Megiddo, "Linear-time algorithms for linear programming in rˆ3 and related problems," *SIAM journal on computing*, vol. 12, no. 4, pp. 759–776, 1983.

[7] B. Gärtner, "Fast and robust smallest enclosing balls," in *European Symposium on Algorithms*. Springer, 1999, pp. 325–338.

[8] J. Kennedy, *Particle Swarm Optimization*. Boston, MA: Springer US, 2010, pp. 760–766.